energies

MDPI

Article

Shale Gas Reservoir Pore Pressure Prediction: A Case Study of the Wufeng–Longmaxi Formations in Sichuan Basin, Southwest China

Or Aimon Brou Koffi Kablan [1,2] and Tongjun Chen [1,2,*]

[1] Laboratory of Resource and Earth Sciences, Ministry of Education, China University of Mining and Technology, Xuzhou 221116, China; fb19010001@cumt.edu.cn
[2] Laboratory of Coalbed Methane Resource and Reservoir Formation Process, Ministry of Education, China University of Mining and Technology, Xuzhou 221008, China
* Correspondence: tjchen@cumt.edu.cn

Abstract: Pore pressure prediction is critical for shale gas reservoir characterization and simulation. The Wufeng–Longmaxi shale, in the southeastern margin of the Sichuan Basin, is identified as a complex reservoir affected by overpressure generation mechanisms and variability in lithification. Thus, standard methods need to be adapted to consistently evaluate pore pressure in this basin. Based on wireline logs, formation pressure tests, and geological data, this study applied the Eaton–Yale approach, which extends the theoretical basis of Eaton and Bowers methods to reservoir geological conditions and basin history. The method was developed by integrating petrophysical properties, rock physics interpretations, and geology information. The essential steps include (1) a multi-mineral analysis to determine mineral and fluid volumes; (2) a determination of the normal pressure trend line and extending it to overpressured sections; (3) predicting pore pressure using the basic Eaton approach and identifying overpressured zones; (4) correcting compressional velocity using lithology logs and a rock physics model; (5) determining the Biot Alpha coefficient and vertical-effective stress and estimating the new pore pressure values using the Eaton–Yale method. Overpressure zones were corrected, and reservoir pore pressure varied between 30.354 and 34.959 MPa in the wells. These research results can provide a basis for building reservoir simulation models, identifying reservoir boundaries, and predicting relative permeability.

Keywords: pore pressure prediction; Eaton–Yale method; shale gas reservoirs; overpressure zones; Sichuan Basin

check for updates

Citation: Kablan, O.A.B.K.; Chen, T. Shale Gas Reservoir Pore Pressure Prediction: A Case Study of the Wufeng–Longmaxi Formations in Sichuan Basin, Southwest China. *Energies* **2023**, *16*, 7280. https://doi.org/10.3390/en16217280

Academic Editor: Reza Rezaee

Received: 5 October 2023
Revised: 16 October 2023
Accepted: 24 October 2023
Published: 26 October 2023

Copyright: © 2023 by the authors. Licensee MDPI, Basel, Switzerland. This article is an open access article distributed under the terms and conditions of the Creative Commons Attribution (CC BY) license (https://creativecommons.org/licenses/by/4.0/).

1. Introduction

Predicting pore pressure is essential for reservoir characterization, evaluation, drilling operations, and exploitation plans. Determining overpressured intervals is challenging because it is a crucial part of offshore basins' geomechanical and geophysical analysis, especially for unconventional hydrocarbon reservoirs [1]. Overpressures in offshore basins are a common phenomenon and can significantly increase drilling time and cause serious incidents such as blowouts and pressure kicks [2,3]. Shale gas exploration is rapidly progressing into complex geological and geophysical settings; thus, systematic procedures to improve exploration and production are essential to support global energy requirements [4]. Consequently, multiple approaches are necessary to integrate geology, geophysics, petrophysics, geomechanics, geostatistics, and reservoir engineering [4–6]. According to the distribution and composition of global resources, the potential reserves of unconventional resources, especially shale gas, are equivalent to conventional gas resources [7]. As an example, China's recoverable shale gas resources comprise about 32 trillion cubic meters, mainly distributed in Sichuan, Ordos, Bohai Bay, Songliao, the middle and lower Yangtze regions, Turpan Hami Basin, Tarim Basin, and Zhungeer Basin [8]. Pore-pressure estimation

in this unconventional natural resource is a significant parameter for global exploration, and its prediction needs to be deeply understood to reduce borehole incidents, correctly estimate reserves, and plan reservoir development [5].

Many research works with different approaches have been proposed in the literature to evaluate pore pressure, with successful results in relatively young basins, North American basins, and clastic formations [4,7,9]. These methods include Hottmann and Johnson pore-pressure prediction [10], which derives pore-pressure from resistivity, or acoustic travel time/velocity, as a function of the burial depth and normal hydrostatic trend. The basic Eaton method [11] calculates pore pressure from sonic compressional transit time or velocity. Eaton assumes that overburden pressure is supported by pore pressure and Terzaghi effective stress principle [12]. The Bowers approach [13] estimates reservoir effective pressure from observed overburden stresses and formation pressure data. The combination of the Bowers approach with the Eaton method is commonly used in the industry. Flemings and Schneider [14,15] applied porosity–stress correlation to determine pore pressure in mudstone formation. The authors used an empirical porosity equation similar to the Eaton approach to predicting pore pressure from shale data. Couzens-Schultz et al. [16] tested the Bowers method in a relatively complex unconventional reservoir and included an evaluation of the cross-plot between vertical-effective stress, shear velocity, and resistivity. Some good pressure results were obtained, but overpressured zones still exist in more complex lithified zones of the studied wells. Xia et al. [17] analyzed pore pressure by addressing the impact of uplift and seal quality on overpressure in unconventional reservoirs. Friedrich and Monson [18] and Rittenhouse et al. [19] used mud-weighted Pad ISIP, DST, DFIT, and ESP data to generate a pore-pressure model from effective stress equation in the Midland basin. Swarbrick et al. [20], Devine [21], and Han et al. [22] analyzed the classic Eaton deviation of compressional slowness (DTC) as an indicator of overpressure and compared it to uplift and DFITs. They observed that the most common source of overpressure in shale gas reservoirs is disequilibrium compaction during sediment loading. Under these conditions, pore pressure can be determined because the relationship between effective stress and porosity is nonexistent. Sayers and Den Boer [23] predicted pore pressure using P-impedance and the ratio of vertical P-velocity to vertical S-velocity (VP/VS) from the inversion of seismic amplitude variation with offset data. The model gives relatively correct results considering lithology and mineralogy influences. However, it is susceptible to unloading effects, changes in rock composition, and vertical seismic resolution.

These empirical methods, essentially based on relationships between different response parameters (well logs, laboratory measurements, and wave velocities), are efficient for relatively young basins where overpressure processes can be minimized. Through the years, most of pore pressure prediction techniques applied in Sichuan Basin were developed for very soft sediments, where the effect of overpressure on velocity differs from fossil sediments. The Wufeng–Longmaxi shale gas reservoirs are complex systems due to compaction mechanisms, formation-tectonic evolution, and lithology variations. These parameters, which vary horizontally and vertically, make it difficult to determine their intrinsic geomechanical properties, particularly pore pressure.

This paper applies a new workflow to the Sichuan Basin shale gas reservoirs. The workflow considers this basin to be relatively old, more lithified, and to have complex tectonics. The study includes bulk modulus, effective stress, and the Eaton–Yale method, which extends the theoretical basis of the Eaton and Bowers methods to unconventional reservoirs, corrects overpressure zones, and considers lithology and mineralogy variations. The method was applied to two wells and validated using formation pressure test results.

2. Geological Setting

The study area is located in the middle of the high and steep fault fold belt east of the Sichuan Basin (Figure 1a), with complex tectonics and strong diagenesis. The target zone is characterized by narrow and steep anticlines accompanied by wide and gentle synclines. The structural plane is represented by a belt distribution along the northeast direction.

Fault distribution is often associated with high structural zones arranged and distributed in the same direction. During the early Silurian period, the euxinic shelf environment dominated the Upper Yangtze area southeast part [24], resulting in a wide deposition of thick organic-rich shale in the southeast Sichuan Basin [25]. The geology is dominated by organic-rich shale and abundant graptolites, and it can be identified as sand-shale (thinly bedded sands and shales) of shallow marine shelf deposits [26,27]. In the regional stratigraphy, the interval includes limestone and mudstone (Figure 1b). An exploration well was drilled vertically using water-based mud to a total measured depth of 2280 m, crossing the Lower Silurian Longmaxi and Upper Ordovician Wufeng formations. General information about the Jiaoshiba shale gas field is presented in Figure 1.

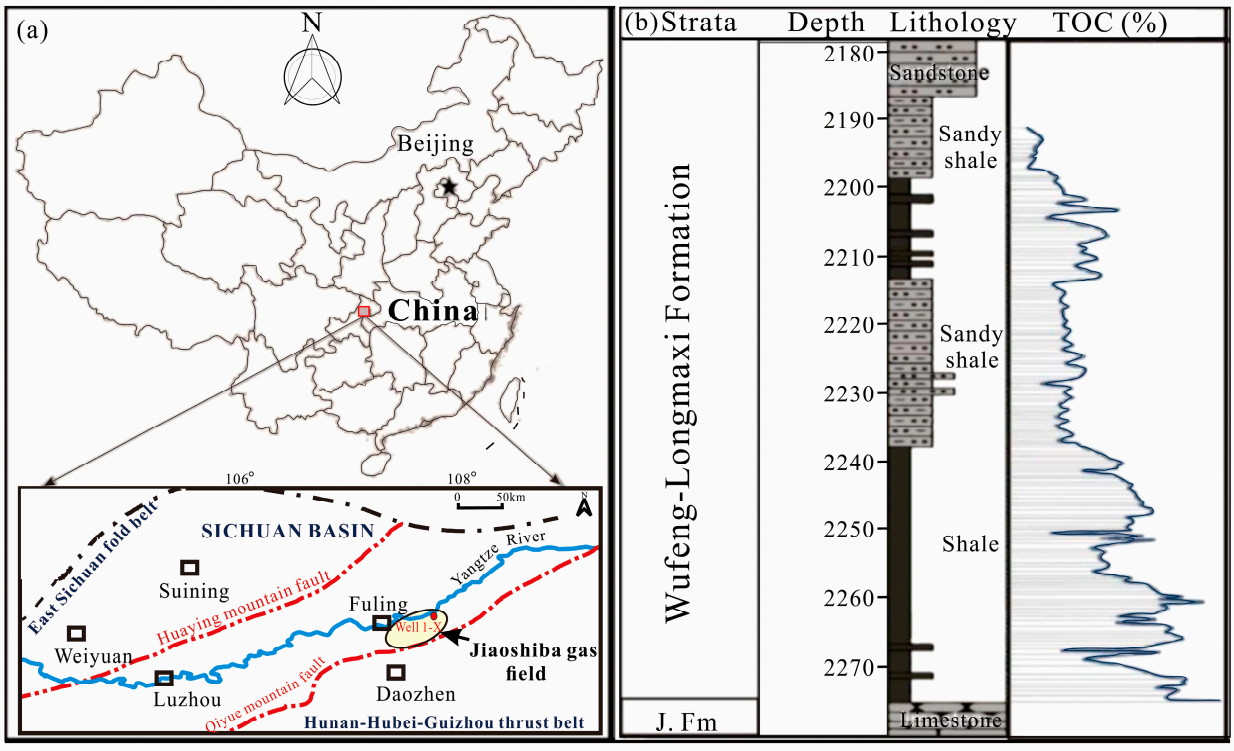

Figure 1. Background information of the Fuling shale gas field: (**a**) location of the study area; (**b**) regional stratigraphy showing strata and lithology. Modified from Chen et al. [5].

3. Methodology

3.1. Data Overview and Workflow

Two wells were used for this study, representing the different zones of the Jiaoshiba shale gas field: well A for shallow sediment zones and well B for deep sediment zones. Available data include conventional wireline logs, geological information, and elastic rock properties. Conventional wireline logs consist of gamma-ray (GR), resistivity (deep and shallow laterologs), spontaneous potential (SP), porosity (density, neutron, and sonic), and acoustic (AC) responses. These data were environmentally adjusted and are consistent for this study. Geological data include daily geological logging, sedimentary facies analysis, lithology identification, and stratification. The formation micro-imager logs (FMI) are available. In situ pressure data from tubing conveyed performing and drill-stem tests (TCP-DST) are available for well A.

The workflow integrates the Eaton–Yale method [2] by extending the theoretical basis of Eaton and Bowers methods, considering lithification and variation in lithology and mineralogy. Bulk modulus (K) and effective stress (S_{eff}) were added to the model to account for the material's elastic properties. Methodologies were implemented in Geolog software 20.0, and the workflow is summarized in Figure 2.

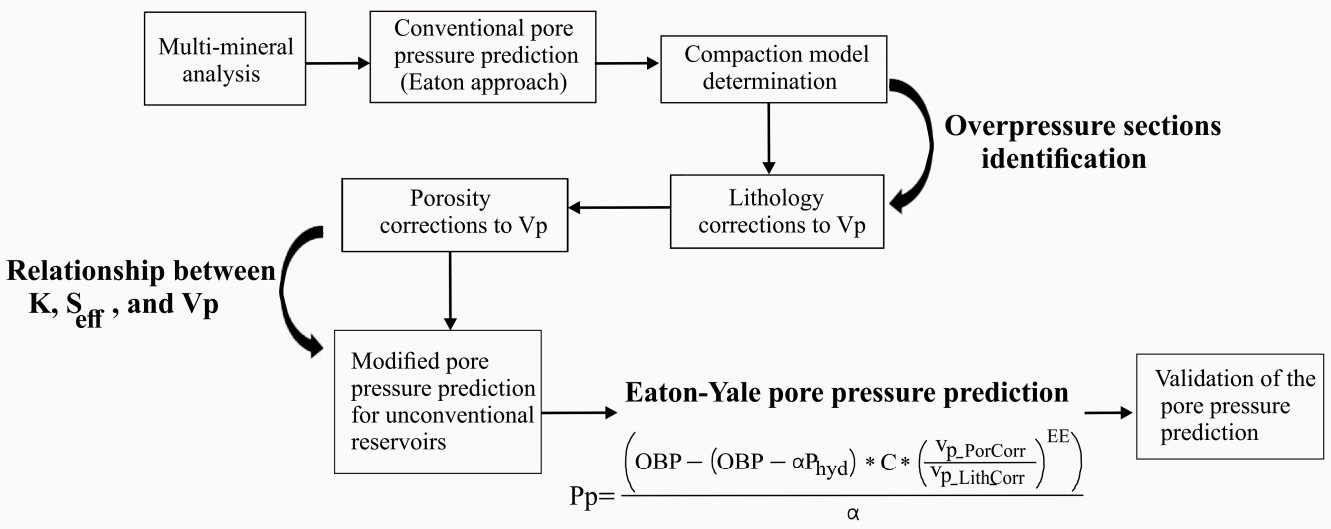

Figure 2. Workflow used for pore pressure prediction.

3.2. Multi-Mineral and Multi-Fluids Analysis

A multi-mineral and fluid analysis (multimin) was used to provide an accurate quantitative evaluation of reservoir petrophysical parameters. The model was built and computed using lithology, mineral interpretation data, and fluid information from wells. The principle is to solve various log-response equations simultaneously to calculate the volumes of multiple minerals and fluids. The multimin optimization model was applied to reduce the non-correlation of the equation matrix by adjusting different input parameters, such as mineral logging response parameters, and solving multiple models according to specific combination probabilities. Predicted logs were adjusted to ensure that the resulting logs were unbiased and accurate.

3.3. Compaction Model

The compaction model main assumption is to consider fluid overpressure caused by disequilibrium compaction and formation variations. Fluid overpressure is the result of a balance between the rate of overpressure generation and its dissipation by fluid flow [28]. Therefore, describing all parameters under hydrostatic conditions is practical because, within this condition, vertical effective stress equations can accurately quantify pore pressures. The cross plot between compressional velocity (Vp) and density (Figure 3) was used to identify this interval, which is one of the trends described by the Swarbrick diagram [29]:

- Trend A: normal compaction trend (overpressure due to disequilibrium).
- Trend B: fluid expansion trend (relatively low increase in density and significant decrease in velocity).
- Trend C: hybrid trend (density increase and velocity decrease).
- Trend D: early chemical diagenesis trend (low increase in velocity and relative density increases).
- Trend E: later diagenetic alteration at high density and low porosity when velocity increases rapidly due to very low porosity.

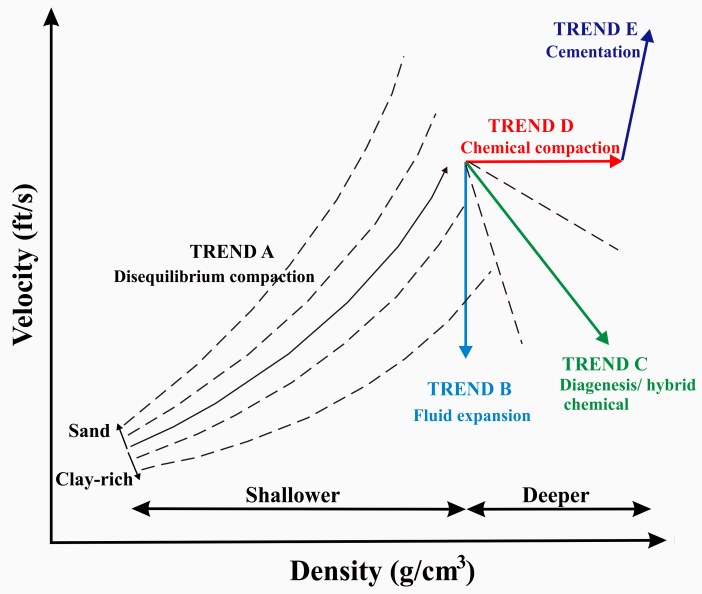

Figure 3. Velocity and density cross plot illustrating the evolution processes of the vertical effective stress. Modified from Swarbrick [29].

In addition, the model includes effective stress (S_{eff}) and bulk modulus (K) characterizations to reflect formations' elastic characteristics and diagenesis. The correlation between these parameters was evaluated based on the logging responses of the measured compressional velocity (Vp), shear velocity (Vs), overburden stress (Sv), pore pressure from Eaton method (Pp), and density (ρ) (Equations (1) and (2)).

$$K = \rho V_P^2 - \frac{4}{3}\rho V_S^2 \tag{1}$$

$$S_{\text{eff}} = S_V - P_P \tag{2}$$

3.4. Standard Eaton Pore Pressure Approach

The standard Eaton method [11] predicts pore pressure from velocity based on drilling parameters and can be determined using the Eaton equation (Equation (3)).

$$P_P = OBP - (OBP - HP) \times \left(\frac{V_{P_meas}}{V_{P_NCT}}\right)^{EE} \tag{3}$$

where Pp is the predicted pore pressure. OBP and HP are the overburden and hydrostatic pore pressures, respectively, caused by weight and fluids. Vp-meas is a measured compressional velocity. Vp-NCT is an extrapolated compressional velocity derived from the normal pressure trend. EE is the Eaton exponent, which equals 4 for old basins. The overburden pressure can be obtained from Terzaghi effective stress principle [12], which is expressed, in this case, by the following Equation (4):

$$OBP = pp + VES \tag{4}$$

where *pp* and *VES* are the intrinsic-matrix pore pressure and matrix-effective vertical stress, respectively. The normal pore pressure trend (NPT) was determined and fitted using Vp as a function of depth to obtain a more realistic NPT curve (Vp-NPT).

3.5. Compressional Modulus Lithology and Porosity Correction

Lithology correction was performed using the Voigt-Reuss-Hill average (VRH) model [30], which calculates the properties of pure mineral constituents in the grain

mixture. Each lithological volume fraction weighs the rock velocity and density to obtain the Vp modulus (Vpmod) of every single mineral (Equation (5)).

$$V_{p\mathrm{mod}} = \rho + V_p^2 \tag{5}$$

where ρis the density of the given mineral, and Vp is the measured compressional velocity

The Vpmod for each mineral in a given mineral assemblage at any given depth was averaged through the VRH model (Equation (6)) to obtain Vpmod-VRH for the mineral assemblage at that depth. The obtained average Vpmod-VRH was compared to the NPT curve-fit section of the well.

$$V_{p\mathrm{mod}_VRH} = \frac{V_{p\mathrm{mod}_1} + V_{p\mathrm{mod}_2}}{2} \tag{6}$$

where $V_{p\mathrm{mod}_1} = f_1 V_{p\mathrm{mod}_meas1}$ and $V_{p\mathrm{mod}_2} = \frac{f_2}{V_{p\mathrm{mod}_meas2}}$.

The terms f_1 and f_2 represent the volume fractions of minerals 1 and 2, respectively. Vpmod_meas1 and Vpmod_meas2 are the Vp moduli measured for minerals 1 and 2, respectively. The Vp-NPT curve was adjusted up or down according to the differences between Vpmod-VRH and Vp-NPT-lithcorr (average Vpmod-VRH of the NPT curve fit section for lithology correction).

Porosity correction was applied using the relationship between porosity and the Vp modulus through the critical porosity method [31], expressed by Equation (7).

$$V_{p\mathrm{mod}} = V_{p\mathrm{mod}_VRH} \times \left(\frac{1-\phi}{\phi_C}\right) \tag{7}$$

where ϕ and ϕ_c are, respectively, the porosity and critical porosity. Vpmod_VRH is the Vp modulus predicted by the VRH average. The critical porosity theory assumes that at zero porosity (ϕ = 0), the Vp modulus of the rock is equal to the Vp modulus predicted by the VRH average of the mineral assemblage (Vpmod = Vpmod_VRH), and the Vp is equal to zero (totally disaggregated rock incapable of supporting acoustic waves) [2]. The adjustment to Vp-measured to obtain a Vp-meas-porocorr was performed to modify Equation (7) to point out the difference in Vpmod between normal porosity and average porosity through the NPT section. This phase is crucial because the Eaton–Yale pore pressure theory determines differences in both lithology and porosity between the normal pressure trend line section and overpressured sections. Thus, the absolute difference between Vp-meas-porocorr and Vp-NPT-lithcorr quantitatively indicates the degree of overpressure.

3.6. Eaton–Yale Pore Pressure Prediction and Validation

The Eaton–Yale method uses the drop in compressional velocities resulting in the change from normal-pressured to overpressured formations due to the lower effective stress and its effect on compressional velocity [2]. This method corrects the variations in porosity and lithology to generate a compressional velocity where overpressure becomes the dominant factor on the corrected velocities (Equation (8)).

$$P_{p\mathrm{mod}} = \left(\frac{OBP - \left(OBP - \alpha P_{hyd}\right) \times C \times \left(\frac{V_{P_PorCorr}}{V_{P_LithCorr}}\right)^{EE}}{\alpha}\right) \tag{8}$$

where Vp-Porcorr is the porosity corrected by the measured Vp, and Vp-LithCorr is the lithology corrected by the Vp-NPT curve. C is a calibration factor equal to 1.1. α, the Biot alpha coefficient, was determined using inversion after adjusting the calibration factor and Eaton exponent.

The calibration was applied during the computation of the Eaton–Yale process in two steps. The first phase consisted of correcting the NPT curve to ensure that the NPT section

was correct, and the second phase was performed by adjusting the calibration factor C and the Eaton exponent EE.

The validation process was accomplished in two ways. The first method evaluated the correlation between effective stress, pore pressure estimated by Eaton–Yale method, and P-velocity. A strong association between these parameters is an indicator of the degree of confidence in the prediction. The second validation method used pressure test data from TCP-DST tests. Results of these tests for well A are available and were performed between 2255.40 and 2314.80 m in the Upper Ordovician Wufeng formation (perforated section: 2304.62–2313.39 m). The test systems were three shut-ins and three shut-offs. The total test time was 340.59 h, including 127.99 h of opening and 212.60 h of shut-ins. The analysis of the recordings was used for validation. As the data are preliminary and incomplete, a process of extrapolation was used for reconstruction and to make them more consistent.

4. Results

Shale gas zones are located in the Wufeng–Longmaxi formation, as shown in Table 1, between 2264.3 and 2363 m for well A and between 2804 and 2898.6 m for well B, respectively, in measured depth (MD).

Table 1. Zonation and geological stratification of gas zones in wells A and B.

Well	Depth Interval (m)	Thickness (m)	Formation
Well A	2264.3–2283.8	19.5	Upper Longmaxi
	2283.8–2356.3	12.5	Lower Longmaxi
	2356.3–2363.0	6.7	Wufeng formation
Well B	2804.0–2817.2	13.2	Upper Longmaxi
	2817.2–2890.0	72.8	Lower Longmaxi
	2890.0–2898.0	8.0	Wufeng formation

The multimin petrophysical model includes the formation composition, conventional logging curves, and mineral logging response. The results of the predicted and corrected logs are presented in Figure 4. The parameters in the tracks are described from the left of the plot. Track 1 contains the estimated mineral composition and corresponding lithology. Corrected porosities and saturation are displayed in tracks 4 and 5. Neutron porosity, gamma ray, density, and photoelectric absorption (PEF) logs are presented in tracks 7, 8, 9, and 10, respectively. Sonic and spontaneous potential (SP) predicted logs are in tracks 11 and 12.

Figure 5 represents the variation between predicted and original log curves associated with the multimin analysis. The general trend was that sensitivities were relatively low in wells A and B. Typically, differences in shallow sediments are relatively high for porosity, fluid saturation, and acoustic logs that change greater than ± 0.02. The change in well B was less than ± 0.03 and between -0.01 and 0.023 for all curves, with higher values for spontaneous potential and fluid saturation. Therefore, the results of log reconstruction indicate that logging quality is good and can accurately reflect the real formation mineral composition, lithology, and pore pressure. The final predicted logs for neutron, gamma ray, density, and PEF were derived from the correlation between the maximum extrapolated log (COR_PLUS) and the minimum predicted log (COR_MIN). The log curves of the study wells appeared consistent, with only minor differences between the initials and the reconstructed curves.

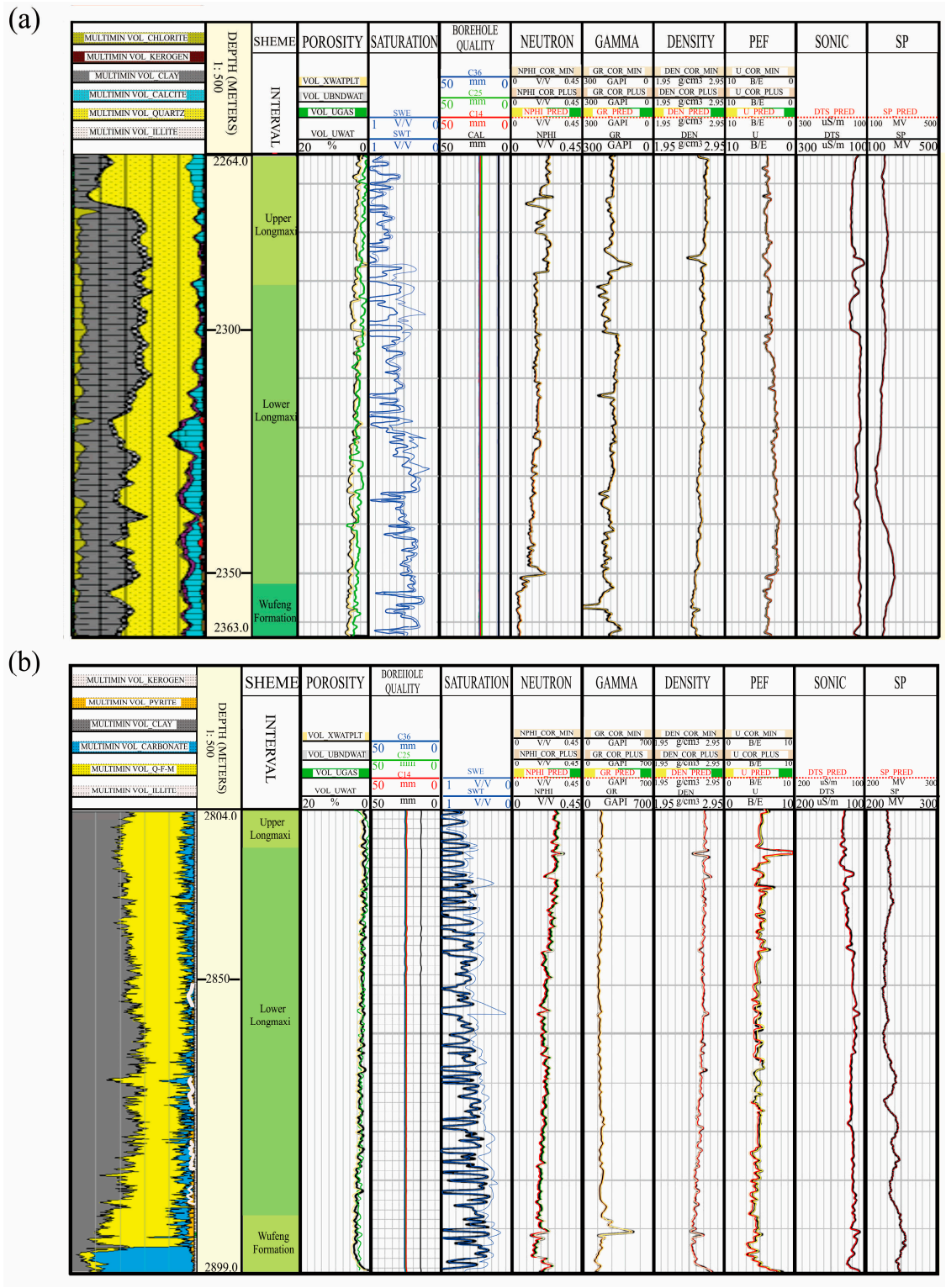

Figure 4. Multi-mineral, multi-fluid analysis, and log reconstructions: (**a**) well A; (**b**) well B. Logs in red represent, for each parameter, the final corrected and predicted log.

Figure 6 shows the compaction evolution in wells A and B. The relative constant trend of Vp and density values identified disequilibrium compaction. Shales at these depth intervals gad densities between 2.55 and 2.65 g/cm^3 for wells A and B. These densities, coupled with the low porosities of these shales ($\phi < 5.0\%$), can ensure that the shales are undrained (in a disequilibrium state).

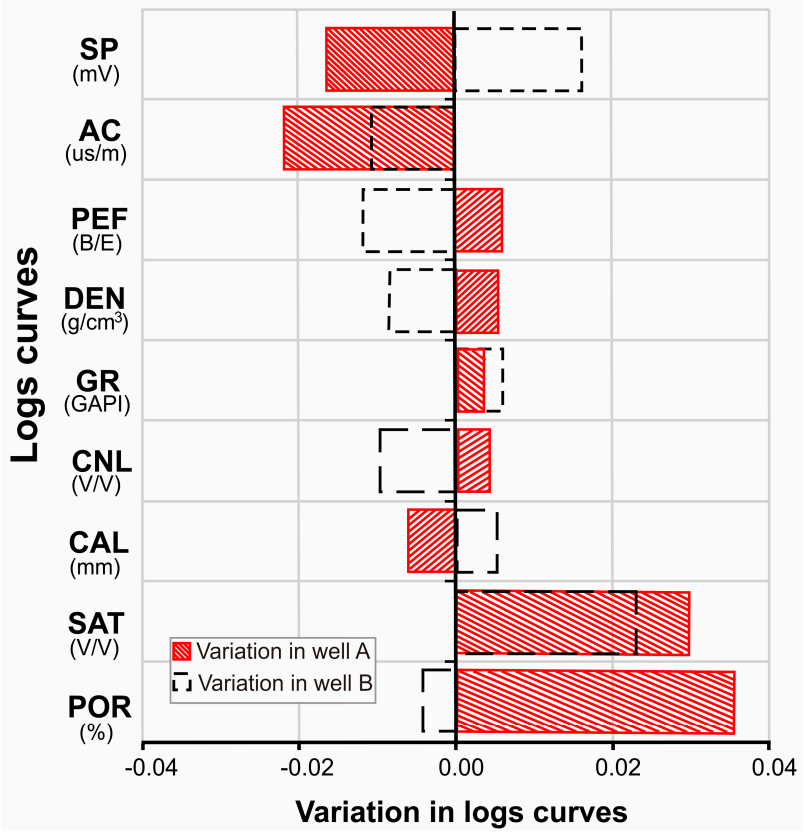

Figure 5. Sensitivity variations between initials and reconstructed curves.

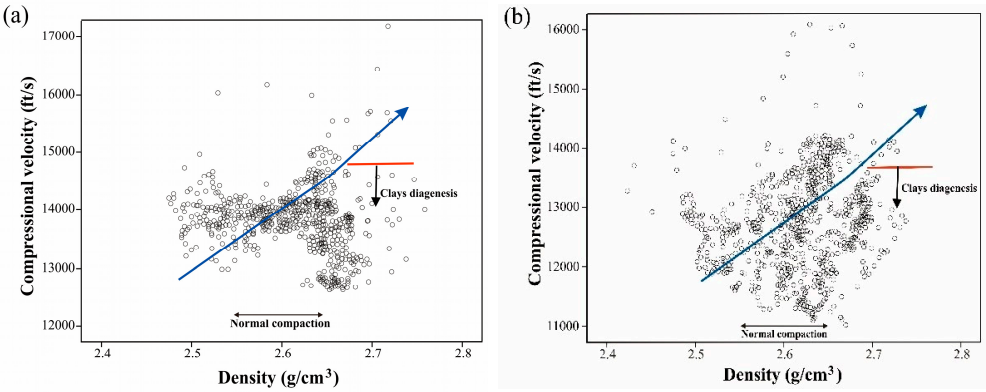

Figure 6. Cross plots between compressional velocity and density showing the compaction evolution in (**a**) well A and (**b**) well B. The blue line represents the normal compaction trend from the Vp (Vp-NCT).

Figure 7 presents the corresponding NPT section of the study wells, from which the NPT curve fit (black line) was derived. The NPT section for curve fitting depends on where the sonic logs start and end. Thus, NPT began at 2275 m and 2805 m, respectively, for wells A and B and ended at 2323 m and 2865 m. A drop in Vp was observed around 2320 m and 2865 m in the wells, corresponding to the middle of the Lower Longmaxi formation. Another Vp decrease due to porosity or lithology changes was observed after 2350 m for well A.

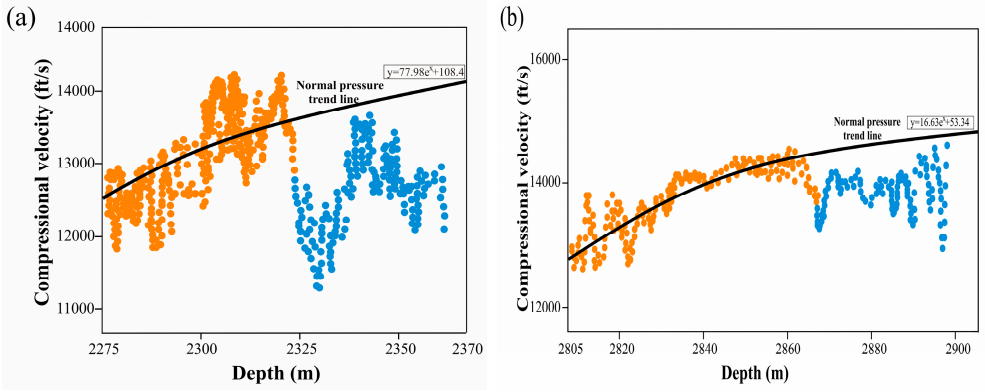

Figure 7. Plots illustrating the normal pressure trend section for compressional velocity curve fit for (**a**) well A and (**b**) well B. The black line represents the normal pressure trend line (NPT), where orange and blue dots indicate the different trends.

Figure 8 presents the results of pore pressure evaluated by the basic Eaton approach and the generated fracture pressure profiles. From the left, track 2 presents the lithology description from comprehensive logging. Track 3 contains the measured compressional velocity (VP) and the extrapolated one from the normal compaction trend (VP_NCT_UNZONED). Track 5 presents hydrostatic pressure (PRESS_HYD), pore pressure from Eaton equation (PRESS_FM_VEL), overburden pressure (PRESS_OB), drilling fluid pressure (PRESS_DF), and fracture pressure (PRESS_FRAC_VEL). The values of these different computed pressures varied between 0 and 100 MPa, and average pore pressure values from the standard Eaton method are detailed in Table 2. Overpressured zones are marked in this table and are indicated in Figure 7 with blue circles.

Table 2. Average pore pressures predicted from the standard Eaton method.

Well A		Well B	
Depth (m)	**PRESS_FM_VEL (MPa)**	**Depths (m)**	**PRESS_FM_VEL (MPa)**
2275–2280	41.834	2805–2810	31.675
2280–2285	32.955	2810–2815	30.172
* **2285–2290**	**41.786**	2815–2820	31.910
2290–2295	29.834	2820–2825	32.172
* **2295–2305**	**40.712**	2825–2835	33.966
2305–2310	30.490	* **2835–2845**	**42.166**
2310–2315	31.982	* **2845–2855**	**48.356**
2315–2323	33.650	2855–2865	33.909

* Overpressure sections.

The measured Vp modulus (ρVp^2) and the Vp modulus calculated from mineral fractions were plotted, and the mineral content section was used to correct the measured rock modulus. This evaluation shows that the study wells sections contained four minerals in different proportions (Table 3), which included siliceous minerals, essentially quartz, carbonates (calcite), clay content (illite), and a proportion of kerogen.

Table 3. Average minerals compositions of the study wells.

Well Name	Calcite (%)	Illite (%)	Quartz (%)	Kerogen (%)
Well A	10.4	34.2	53.4	2.0
Well B	10.0	50.0	35.0	5.0

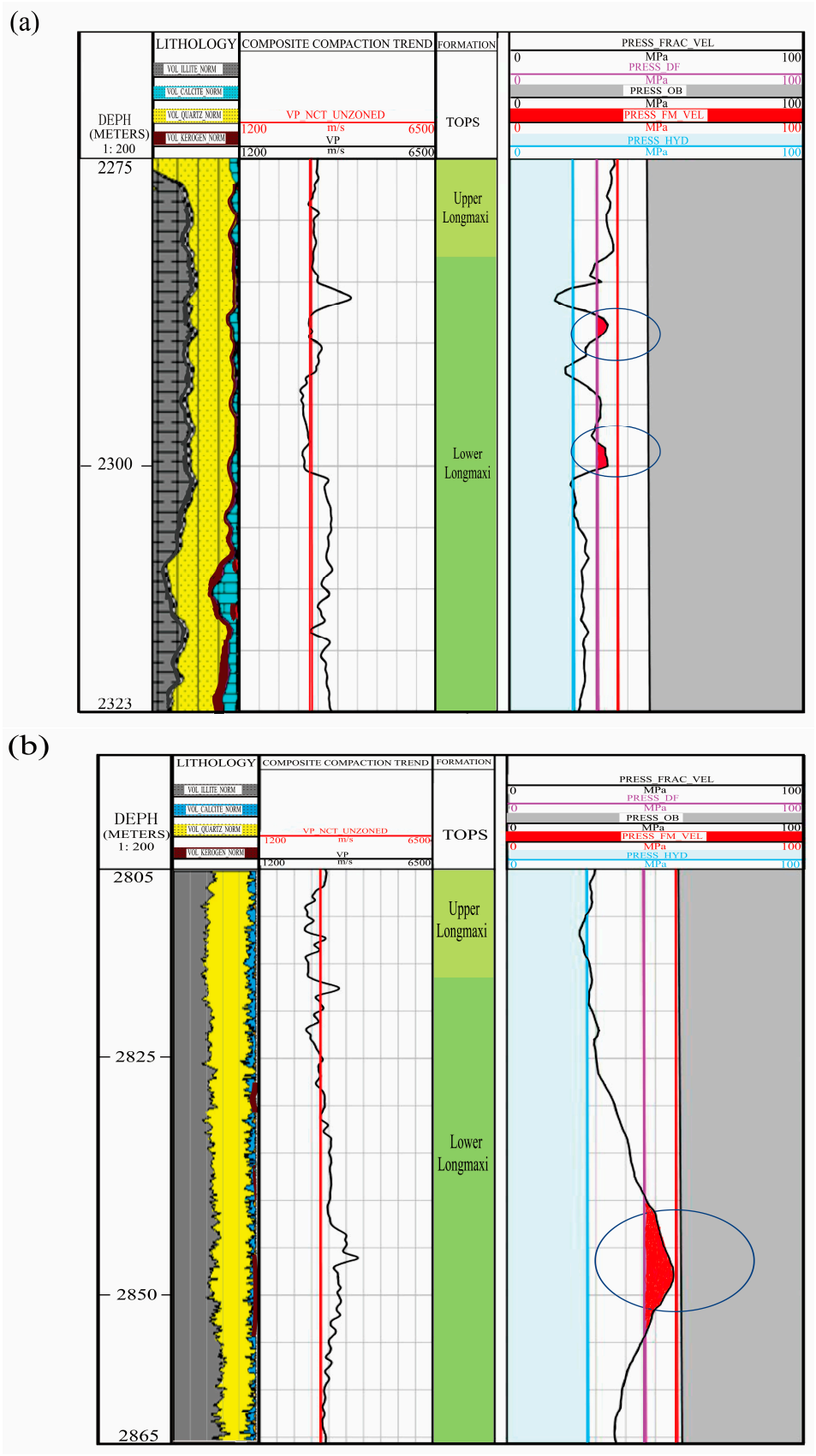

Figure 8. Pore pressure, fractures, and overburden gradients estimated in (**a**) the shallow sediments (well A) and (**b**) deep sediments (well B). The zones circled (in blue) represent the overpressured areas of the wells.

The properties of each constituent are illustrated in Table 4, and the compressional modulus was corrected by applying the normal VRH average to compressional modulus of each mineral depth. Velocity increased with calcite content and decreased with the presence of kerogen in the formation.

Table 4. Physical characteristics of each constituent [30].

Rock Composition	P-Velocity (m/s)	S-Velocity (kg/m^3)	Density (kg/m^3)	Compressional Modulus (MPa)
Calcite	6377.6	3534	2710	110,220
Illite	3571.4	2100	2780	35,450
Quartz	6047.8	4118	2650	96,920
Kerogen	2381.3	1200	1300	7370

Figure 9 shows the result of the lithology correction and points out its importance in this study. From the left, track 2 presents a lithology description, including the principal constituents in their relative proportions in the mixture. Measured compressional modulus from elastic properties (MMOD) and corrected compressional modulus by mineral fractions via the VRH rock physics model (MMOD_LITH_CORR) are displayed in track 3. The velocity-normal compaction trend line is represented in this track (straight black line). Track 4 contains normal compressional velocity (VP) and velocity corrected by lithology (VP_LITH_CORR). Track 6 shows the normal compressional velocity (VP) and velocity corrected by rock physics (VP_PORCORR). The measured compressional moduli and compressional velocities in wells A and B are lower than the corrected values. These differences are due to the simultaneous effects of minerals porosity and grain contact. A significant drop in measured Vp was observed with each increase in formation porosity in deep sediments compared to shallow sediments.

Figure 10 presents the cross plots between S_{eff}, V_P, and K, indicating a good correlation, with coefficients equal to 0.81 and 0.79 for wells A and B, respectively. A linear polynomial function was associated with each correlation, and the corresponding fitted coefficients were identified. For practical use, 2D cross plots are displayed, on which the bulk modulus (colors and trend lines), V_P (x-axis), and effective stress (y-axis) are indicated. With this positive and relatively high association, which integrates the physical properties of the rock, reservoir overpressure zones of the target shale can be reliably corrected using the Eaton–Yale method.

Pore pressure values obtained from the Eaton–Yale method are illustrated in Figure 11 and Table 5, where the precedent overpressured zones, which are now corrected, are marked. Track 3 includes pore pressures predicted by the Eaton–Yale method (PPP_UNCONVEN_UNZONED) and previously calculated pressures. The new values of pore pressures varied between 30 and 35 MPa for both deep and shallow sediment reservoirs.

A good relationship was identified for the correlation between S_{eff}, Pp, and Vp, with coefficients of 0.82 and 0.85 for wells A and B, respectively (Figure 12). These strong associations suggest a high degree of confidence of more than 80% in the pore pressure estimation, which is acceptable for this study given the complexity of this basin.

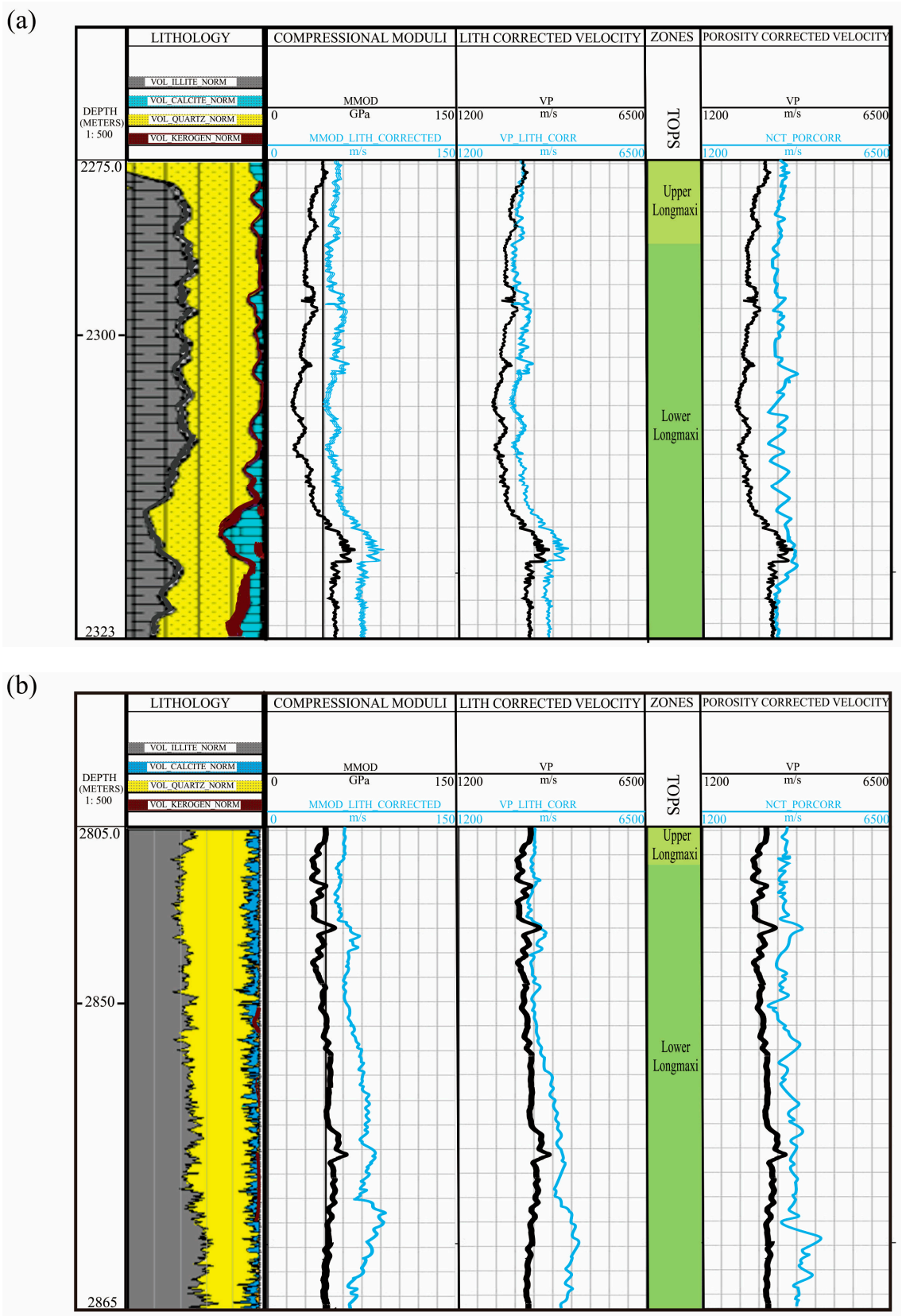

Figure 9. Display of the measured and corrected compressional moduli, lithology, and velocity logs in (**a**) well A and (**b**) well B. For each parameter, the measured log is in black, and the corrected is represented in blue.

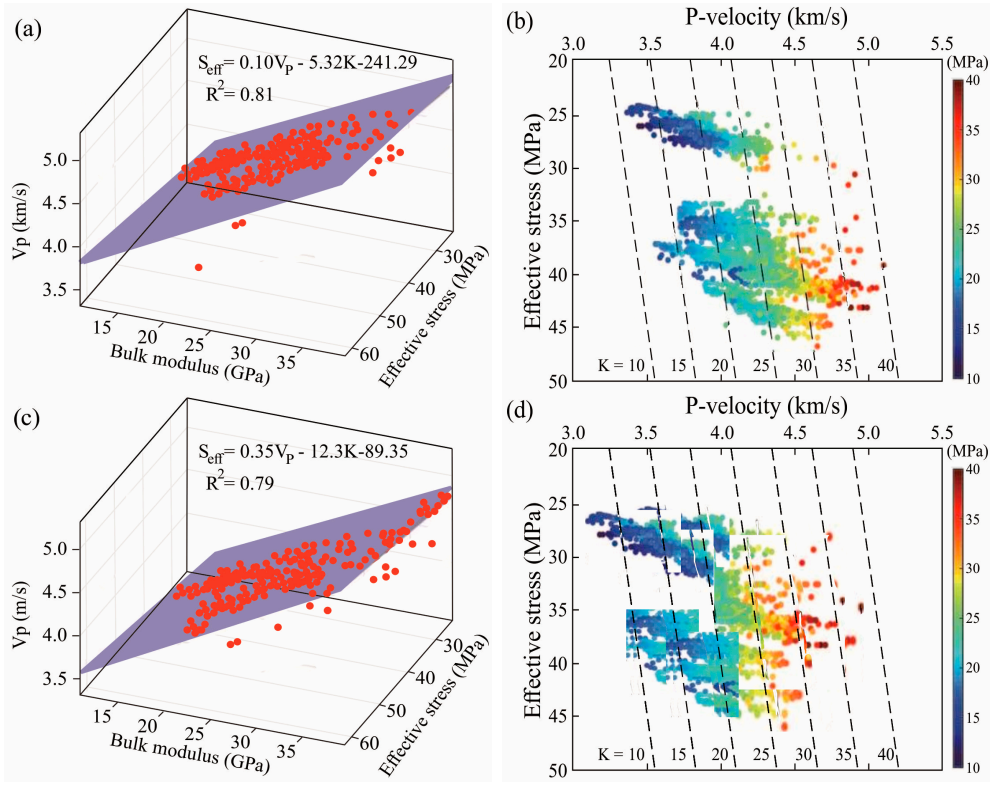

Figure 10. Correlation between S_{eff}, V_P, and K: (**a**,**b**) 3D and 2D cross plots for well A; (**c**,**d**) 3D and 2D cross plots for well B.

Table 5. Average pore pressures predicted from the Eaton–Yale method.

Well A		Well B	
Depths (m)	**PRESS_FM_VEL (MPa)**	**Depths (m)**	**PRESS_FM_VEL (MPa)**
2275–2280	33.450	2805–2810	31.545
2280–2285	33.955	2810–2815	32.296
* **2285–2290**	**32.631**	2815–2820	32.974
2290–2295	30.354	2820–2825	32.172
* **2295–2305**	**33.962**	2825–2835	33.958
2305–2310	32.043	* **2835–2845**	**34.091**
2310–2315	33.225	* **2845–2855**	**34.959**
2315–2323	32.056	2855–2865	33.017

* Corrected overpressure sections.

The TCP-DST test results for well A are presented in Table 6. The control joint pressure was 26.94 MPa, and the maximum recovery semi-logarithmic extrapolation pressure was measured at 2362.60 m with a value of 29.65 MPa. The maximum fitting pressure was 33.62 MPa. Through the fitting pressure, the middle of the formation (2360.10 m) was 32.31 MPa. A comparison of the data from TCP-DST and the Eaton–Yale method indicated two trends. Below 2306 m, pressure values predicted by Eaton–Yale method appeared to be lower than those measured by TCP-DST. Beyond this depth, this trend was reversed (Figure 13). These differences were expected due to unstable recovery pressure and limited shut-in time. Although, for both cases, these differences are ±2 MPa, which can be considered acceptable.

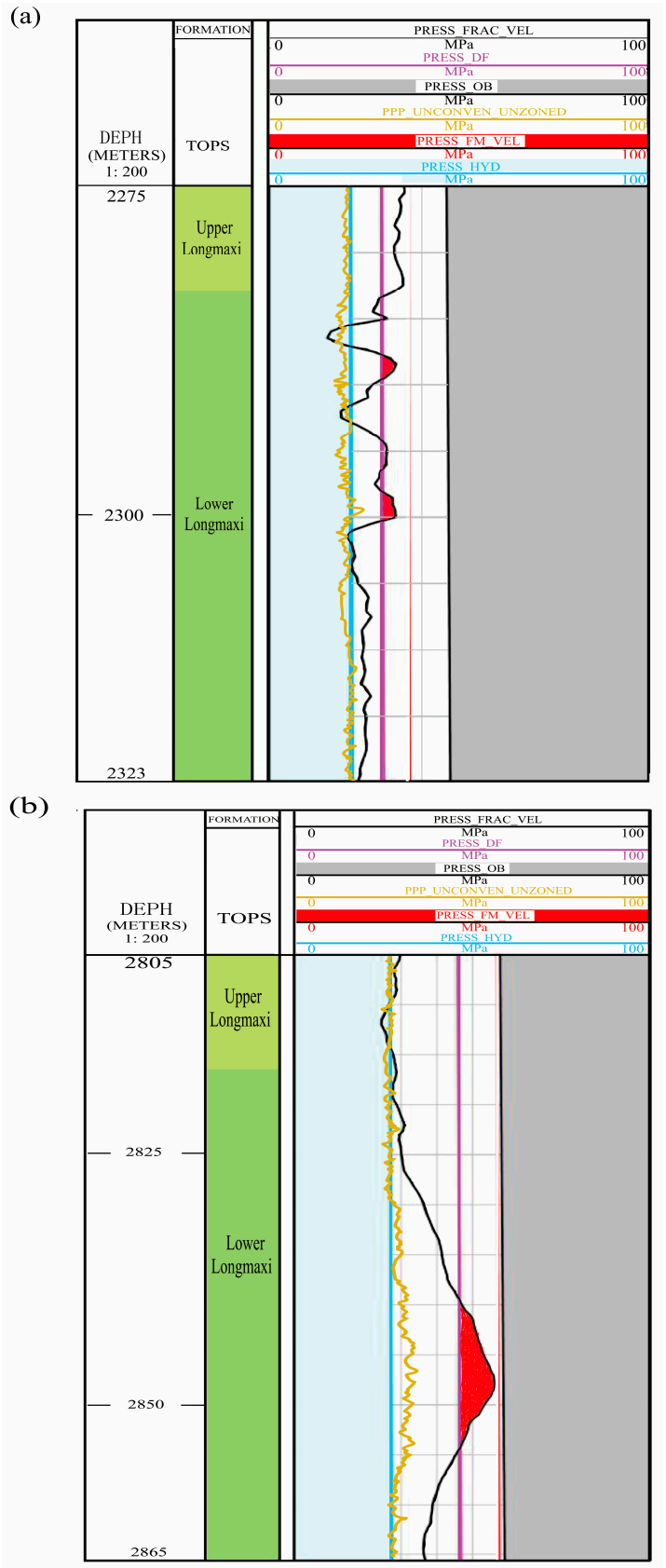

Figure 11. Pore pressure from the Eaton–Yale method and previously estimated pressures showing the entire section of (**a**) well A and (**b**) well B.

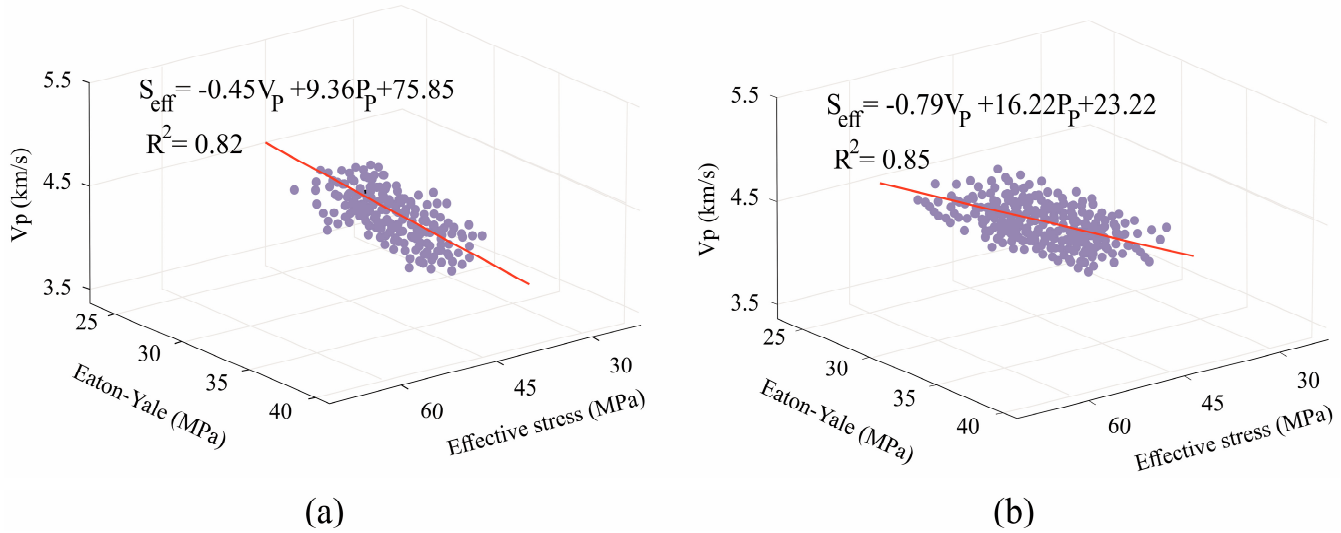

Figure 12. Three-dimensional cross plots showing the correlation between S_{eff}, Pp, and Vp for (**a**) well A and (**b**) well B.

Table 6. TCP-DST results of well A.

Time	Depth (m)	Operations	Semi-Logarithmique Extrapolation Pressure (MPa)	Fitting Pressure (MPa)	Temperature (°C)
17: 05	-	Circulation started	-	-	-
07: 00	-	Circulation stopped	-	-	-
13:00	2304.62	Shut 1	26.94	31.85	79.89
17:00	2308.10	Shut 2	28.15	32.31	82.98
23:00	2313.39	Shut 3	29.65	33.62	86.58

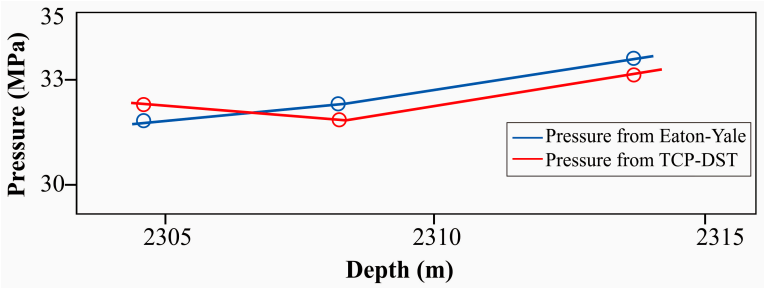

Figure 13. Comparison between pressure from the Eaton–Yale method and TCP-DST tests for well A.

5. Discussion

5.1. Comparative Evaluation of the Proposed Workflow

The Eaton–Yale pore-pressure prediction results were compared to some traditional methods. The most commonly used methods include the basic Eaton method, the Traugott method [32], and the Flemings approach [14]. Whereas the Eaton method is a prediction method based on a velocity trend line, the Traugott and Flemings methods are based on a porosity trend line. Pore pressures from the above approaches were predicted for well A, and calculation results show overpressure in some depth zones. The Eaton–Yale method is independent of internal factors in the well, whereas the other three methods present overpressure zones due to the diagenesis effect. The basic Eaton and Flemings methods have, in most cases, the same values and vary less with lithology change based on

petrophysical interpretation [25]. In contrast, the pore pressure estimated by the Traugott method was relatively higher compared to the values calculated with the Flemings method, varying between 26 and 45 MPa. Compared with drilling fluid density, the results of Eaton–Yale method were more consistent than those of the basic Eaton, Flemings, and Traugott methods (Figure 14). Therefore, the effectiveness of these methods needs to be considered before applying them to the Sichuan Basin; overpressure needs to be addressed. In summary, the proposed workflow, including the Eaton–Yale method, provides reliable results and could accurately help determine pore pressure in the Sichuan basin without extensive testing.

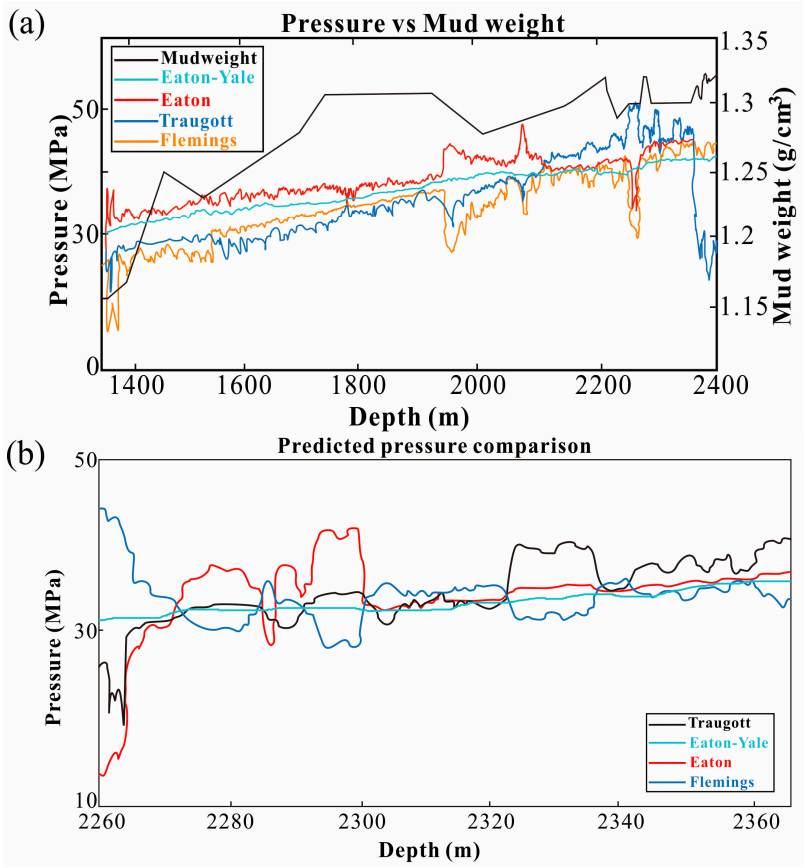

Figure 14. Pore pressure prediction using the Eaton–Yale, standard Eaton, Traugott, and Flemings methods in well A: (**a**) comparison with the drilling fluid density; (**b**) predicted pore pressure between 2260 and 2360 m.

5.2. Limitations and Validation of the Eaton–Yale Approach

The Eaton–Yale method is sensitive and depends on lithological correction and compressional velocity. Thus, higher confidence in the petrophysical model is crucial for this method. The results show that when using accurate rock modeling and a good set of calibration data, the process has a stronger theoretical foundation and gives reliable results. In contrast, when some well data or geological information are missed, the results can be biased. Another fundamental aspect of the Eaton–Yale method is validation. This method requires validation points and is sensitive to this aspect due to sediment lithification and variations in burial depths [2]. For a series of wells in a basin, validation can be accomplished using compressional velocity and by determining the inverted compressional velocity. In this case, the estimated pore pressure gradient trend has opposite distribution characteristics to the inverted compressional velocity, which is consistent with the effective stress theory [1,30]. Therefore, this approach can be helpful when applying the Eaton–Yale process on a basin scale. An example is given in Figure 15, which represents

this observation in some wells (designated from A to G) of the study area. The P-velocity values increased from left to right (Figure 15a); in contrast, the pore pressure gradient (PPG) decreased from left to right (Figure 15b). Considering that TCP-DST pressure test data are, in most cases, incomplete or limited in quantity, this technique can be used for a given set of wells as a method for verification and validation.

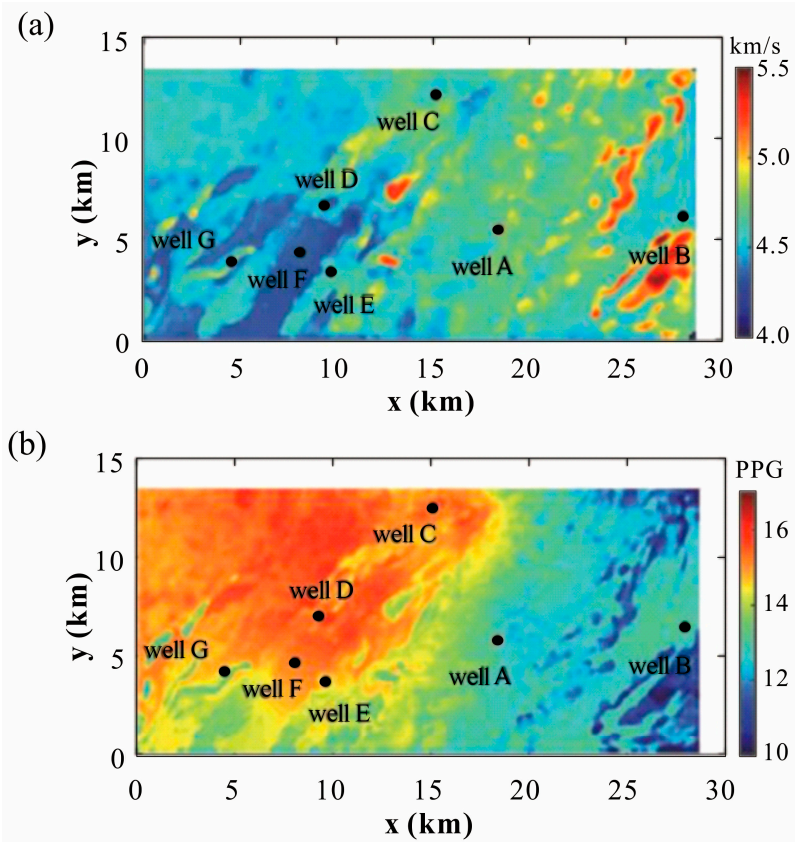

Figure 15. General seismic mapping of the study area: (**a**) inverted compressional velocity; (**b**) predicted pore pressure gradient of the target shale.

6. Conclusions

Pore pressure analysis of the Wufeng–Longmaxi gas reservoir in the Sichuan Basin was performed using wireline logs, geology interpretation, and pressure test results. The study identified overpressure zones and applied the Eaton–Yale pore pressure method to the reservoir, considering variations in the formations' elastic properties. The proposed workflow presents a practical prediction approach using a modification of the Eaton velocity-effective stress method, which considers the significant variations of lithology, porosity, and inorganic mineralogy encountered in the reservoir. Disequilibrium compaction and variations in mineralogy were supposed to be the principal causes of overpressure within the reservoir, and using a rock physics model, the approach corrects variations in porosity and mineralogy to generate a corrected sonic velocity. The effects of density in mud rock and organic minerals, essentially TOC and kerogen, were included in the model to reflect the basin geological history. The results of this model applied to wells are more accurate and consistent with the measured TCP-DST pressure tests compared to traditional methods. The measured pressures in these wells show overpressure zones between the reservoir layers. The research results can provide a basis for modeling rock properties, building a reservoir simulation model, and determining relative permeability. Further studies can integrate a comprehensive seismic model investigation to reduce uncertainties.

Author Contributions: Conceptualization, O.A.B.K.K.; methodology, T.C. and O.A.B.K.K.; software, O.A.B.K.K.; validation, T.C.; investigation, O.A.B.K.K.; resources, T.C.; data curation, T.C.; writing—original draft preparation, O.A.B.K.K.; writing—review and editing, T.C.; visualization, O.A.B.K.K.; supervision, T.C.; funding acquisition, T.C. All authors have read and agreed to the published version of the manuscript.

Funding: This research was funded by the National Key Research and Development Project of China, grant number 2021YFC2902003, and a project funded by the Priority Academic Program Development of Jiangsu higher education institutions.

Data Availability Statement: Not applicable.

Conflicts of Interest: The authors declare no conflict of interest.

References

1. Bahmaei, Z.; Hosseini, E. Pore pressure prediction using seismic velocity modeling: Case study, Sefid-Zakhor gas field in Southern Iran. *J. Pet. Explor. Prod. Technol.* **2020**, *10*, 1051–1062. [CrossRef]
2. Yale, D.P.; Perez, A.; Raney, R. Novel pore pressure prediction technique for unconventional reservoirs. In Proceedings of the SPE/AAPG/SEG Unconventional Resources Technology Conference, Houston, TX, USA, 23 July 2018.
3. Lei, T.; Yin, X.; Zong, Z. Pore pressure prediction in orthotropic medium based on rock physics modeling of shale gas. *J. Nat. Gas Sci. Eng.* **2020**, *74*, 103091. [CrossRef]
4. Dong, D.; Liang, F.; Guan, Q.; Jiang, Y.; Zhou, S.; Yu, R.; Gu, Y.; Zhang, S.; Qi, L.; Liu, Y. Development model and identification of evaluation technology for Wufeng Formation–Longmaxi Formation quality shale gas reservoirs in the Sichuan Basin. *Nat. Gas. Ind. B* **2023**, *10*, 165–182. [CrossRef]
5. Chen, T.; Mukerji, T.; Ma, G.; Wei, Y.; Jin, J.; Song, X. Pore Pressure Prediction for a Paleozoic Marine Shale in South China. In Proceedings of the 81st EAGE Conference and Exhibition, London, UK, 3–6 June 2019.
6. Mgimba, M.M.; Jiang, S.; Mwakipunda, G.C. The identification of normal to underpressured formations in the Southeastern Sichuan basin. *J. Pet. Sci. Eng.* **2022**, *219*, 111085. [CrossRef]
7. Liu, R.; Zheng, J.; Hao, F.; Nie, Z.; Heng, D.; Tan, X.; Jiang, D. Variation in pore systems with tectonic stress in the overthrust Wufeng-Longmaxi shale of the southern Sichuan Basin, China. *J. Nat. Gas Sci. Eng.* **2020**, *83*, 103617. [CrossRef]
8. Sun, C.; Nie, H.; Dang, W.; Chen, Q.; Zhang, G.; Li, W.; Lu, Z. Shale gas exploration and development in China: Current status, geological challenges, and future directions. *Energy Fuels* **2021**, *35*, 6359–6379. [CrossRef]
9. Das, B.; Chatterjee, R. Mapping of pore pressure, in-situ stress and brittleness in unconventional shale reservoir of Krishna-Godavari basin. *J. Nat. Gas Sci. Eng.* **2018**, *50*, 74–89. [CrossRef]
10. Hottmann, C.E.; Johnson, R.K. Estimation of formation pressures from log-derived shale properties. *J. Pet. Technol.* **1965**, *17*, 717–722. [CrossRef]
11. Eaton, B.A. The equation for geopressure prediction from well logs. In Proceedings of the SPE Annual Technical Conference and Exhibition, Dallas, TX, USA, 28 September 1975.
12. Terzaghi, K.; Peck, R.B.; Mesri, G. *Soil Mechanics in Engineering Practice*, 1st ed.; John Wiley & Sons: Hoboken, NJ, USA, 1996; pp. 44–53.
13. Bowers, G.L. Pore pressure estimation from velocity data: Accounting for overpressure mechanisms besides undercompaction. *SPE Drill. Complet.* **1995**, *10*, 89–95. [CrossRef]
14. Flemings, P.B.; Stump, B.B.; Finkbeiner, T.; Zoback, M. Flow focusing in overpressured sandstones: Theory, observations, and applications. *Am. J. Sci.* **2002**, *302*, 827–855. [CrossRef]
15. Schneider, J.; Flemings, P.B.; Dugan, B.; Long, H.; Germaine, J.T. Overpressure and consolidation near the seafloor of Brazos-Trinity Basin IV, northwest deepwater Gulf of Mexico. *J. Geophys. Res. Solid.* **2009**, *114*. [CrossRef]
16. Couzens-Schultz, B.A.; Axon, A.; Azbel, K.; Haugland, M.; Sarker, R.; Tichelaar, B.; Wiesneck, J.B.; Wilheml, R.; Zhang, J.; Zhang, Z. Pore pressure prediction in unconventional resources. In Proceedings of the International Petroleum Technology Conference, Beijing, China, 26 March 2013.
17. Xia, X.; Wallace, J.; Du, L. Modeling of abnormal fluid pressure in unconventional plays due to uplift. In Proceedings of the SPE/AAPG/SEG Unconventional Resources Technology Conference, Denver, CO, USA, 12–14 August 2013.
18. Friedrich, M.; Monson, G. Two practical methods to determine pore pressure regimes in the Spraberry and Wolfcamp formations in the Midland basin. In Proceedings of the Unconventional Resources Technology Conference, Denver, CO, USA, 12–14 August 2013.
19. Rittenhouse, S.; Currie, J.; Blumstein, R. Using mud weights, DST, and DFIT data to generate a regional pore pressure model for the Delaware Basin, New Mexico and Texas. In Proceedings of the Unconventional Resources Technology Conference, San Antonio, TX, USA, 1–3 August 2013.
20. Swarbrick, R.; Lahann, R.; O'Connor, S.; Hoskin, E. Limitations of seismic pore pressure prediction-what is the alternative? In Proceedings of the 75th EAGE Conference & Exhibition-Workshops, London, UK, 10 June 2013.

21. Devine, P.E. Toward Understanding Over-Pressure in a Basin with Burial and Uplift: Preliminary Results of a Study Measuring Under-Compaction with DT Logs. In Proceedings of the Unconventional Resources Technology Conference, Denver, CO, USA, 25–27 August 2014.
22. Han, T.; Pervukhina, M.; Ben Clennell, M.; Neil Dewhurst, D. Model-based pore-pressure prediction in shales: An example from the Gulf of Mexico, North America. *Geophysics* **2017**, *82*, M37–M42. [CrossRef]
23. Sayers, C.; Den Boer, L. Seismic pore pressure estimation in unconventional reservoirs. In Proceedings of the Second EAGE/AMGP/AMGE Latin American Seminar in Unconventional Resources, Mexico City, Mexico, 14–15 November 2019.
24. Liang, Z.; Jiang, Z.; Wu, W.; Guo, J.; Wang, M.; Nie, Z.; Li, Z.; Xu, D.; Xue, Z.; Chen, R.; et al. Study and Classification of Porosity Stress Sensitivity in Shale Gas Reservoirs Based on Experiments and Optimized Support Vector Machine Algorithm for the Silurian Longmaxi Shale in the Southern Sichuan Basin, China. *ACS Omega* **2022**, *7*, 33167–33185. [CrossRef] [PubMed]
25. Zhang, J.; Zheng, H.; Wang, G.; Liu, Z.; Qi, Y.; Huang, Z.; Fan, X. In-situ stresses, abnormal pore pressures and their impacts on the Triassic Xujiahe reservoirs in tectonically active western Sichuan basin. *Mar. Pet. Geol.* **2020**, *122*, 104708. [CrossRef]
26. Ou, C.; Li, C.; Rui, Z.; Ma, Q. Lithofacies distribution and gas-controlling characteristics of the Wufeng–Longmaxi black shales in the southeastern region of the Sichuan Basin, China. *J. Pet. Sci. Eng.* **2018**, *165*, 269–283. [CrossRef]
27. Shu, Y.; Lu, Y.; Chen, L.; Wang, C.; Zhang, B. Factors influencing shale gas accumulation in the lower Silurian Longmaxi formation between the north and South Jiaoshiba area, Southeast Sichuan Basin, China. *Mar. Pet. Geol.* **2020**, *11*, 905–917. [CrossRef]
28. Urpi, L.; Rinaldi, A.P.; Rutqvist, J.; Wiemer, S. Fault stability perturbation by thermal pressurization and stress transfer around a deep geological repository in a clay formation. *J. Geophys. Res. Solid. Earth* **2019**, *124*, 8506–8518. [CrossRef]
29. Swarbrick, R. Review of pore-pressure prediction challenges in high-temperature areas. *Lead. Edge* **2012**, *31*, 1288–1294. [CrossRef]
30. Mavko, G.; Mukerji, T.; Dvorkin, J. *The Rock Physics Handbook*, 3rd ed.; Cambridge University Press: Cambridge, UK, 2020; pp. 345–351.
31. Vernik, L. *Seismic Petrophysics in Quantitative Interpretation*; Society of Exploration Geophysicists: Houston, TX, USA, 2016; pp. 145–153.
32. Traugott, M. Pore/fracture pressure determinations in deep water. *World Oil* **1997**, *218*, 68–70.

Disclaimer/Publisher's Note: The statements, opinions and data contained in all publications are solely those of the individual author(s) and contributor(s) and not of MDPI and/or the editor(s). MDPI and/or the editor(s) disclaim responsibility for any injury to people or property resulting from any ideas, methods, instructions or products referred to in the content.